JOURNAL OF SOLID STATE CHEMISTRY 58, 350–356 (1985)

New Cesium Titanate Layer Structures

I. E. GREY, I. C. MADSEN, AND J. A. WATTS

CSIRO Division of Mineral Chemistry, P.O. Box 124, Port Melbourne, Victoria, Australia 3207

AND L. A. BURSILL AND J. KWIATKOWSKA

School of Physics, University of Melbourne, Parkville, Victoria, Australia 3052

Received August 17, 1984; in revised form December 28, 1984

A phase study of the Cs_2O–TiO_2 system in the composition range 75–100 mole% TiO_2 and the temperature range 850–1200°C revealed the existence of two new cesium titanates, with compositions $Cs_2Ti_5O_{11}$ and $Cs_2Ti_6O_{13}$. The former compound undergoes a reversible hydration reaction below 200°C to form $Cs_2Ti_5O_{11} \cdot (1 + x)H_2O$, $0.5 < x < 1$. The structures of the three phases have been determined. They are based on corrugated layers of edge-shared octahedra, with cesium ions (and H_2O) packing between the layers. In $Cs_2Ti_6O_{13}$, the layers are continuous in two dimensions, whereas in $Cs_2Ti_5O_{11}$ and $Cs_2Ti_5O_{11} \cdot (1 + x)H_2O$, the layers are periodically stepped to give 5-octahedra wide, corner-linked ribbons.

Introduction

The incorporation of cesium in crystalline titanate phases is of current interest (*1–4*) in the search for suitable host matrices for safe disposal of high-level radioactive waste. The synthetic phase mixtures that have received the most attention are the SYNROC assemblages, comprising the minerals perovskite, zirconolite, and hollandite (*5*). Cesium is thought to be incorporated in the Ba-hollandite phase, $BaAl_2Ti_6O_{16}$ (*5*).

A recent study of cesium incorporation in the hollandite-related phase, $Ba_2Ti_9O_{20}$, showed only limited solid solubility, with unmixing into $Ba_2Ti_9O_{20}$ and a cesium titanate at temperatures above 1150°C (*4*). The characterization of the new cesium titanate led to a more general study of the stability and structures of phases in the Cs_2O–TiO_2 system, the results of which are reported here.

Experimental

Starting materials for the phase study were Fisher-certified TiO_2 (anatase form) and analytical reagent grade $CsNO_3$ (BDH). Weighed samples of the two compounds were intimately mixed and ground, pressed into ¼-in. diameter pellets, and calcined in air at 850°C to decompose the nitrate. Heat treatments were performed at 850–1200°C for times from 2 to 100 hr, followed by rapid cooling in air to ambient temperature. Reacted samples were usually ground, repelleted, and given a second heat treatment. For

0022-4596/85 $3.00

some samples, the pellets were contained within platinum crucibles and the weight change monitored as a function of heating time, to measure the rate of volatilization of cesium.

A series of sealed-tube reactions was carried out, using TiO_2 and CsOH (Koch Light, 99%) as starting reagents. These were ground and mixed in a nitrogen-filled glovebag and transferred to platinum tubes which were sealed with a carbon-arc. The tubes were tested for leaks by boiling in water, then sealed within evacuated silica tubes. The samples were held overnight at 300°C (mp of CsOH = 272°C), before raising to the reaction temperature.

The phases in the reaction products were identified from powder XRD patterns taken with a Philips diffractometer fitted with a graphite monochromator and employing Cu$K\alpha$ radiation. For lattice parameter determinations, corundum was added as an internal standard and a scan rate of $\frac{1}{2}°$ 2θ min^{-1} was used. Powder patterns at elevated temperatures were obtained using a Rigaku theta-theta high-temperature diffractometer, with automatic temperature programmer. Unit cell parameters and space groups were confirmed using both single-crystal XRD (precession and Weissenberg methods) and selected-area electron diffraction techniques (JEOL-100 CX electron microscope, operated at 100 kV). Weissenberg XRD patterns were obtained at elevated temperatures by blowing hot helium gas onto the crystal, held in place with silicone cement (SILASTIC, Dow Corning Corp.).

Simultaneous thermogravimetry and differential thermal analysis measurements were recorded with a Stanton Redcroft STA-780 thermal analyzer. About 20-mg samples were heated in a static air atmosphere at a rate of 10° min^{-1} using alumina as reference material.

Infrared spectra were recorded for the samples in KBr disks using a Digilab FTS-20 Fourier-transform infrared spectrometer. Fifty scans were acquired in the region 4000–500 cm^{-1} at a resolution of 4 cm^{-1}.

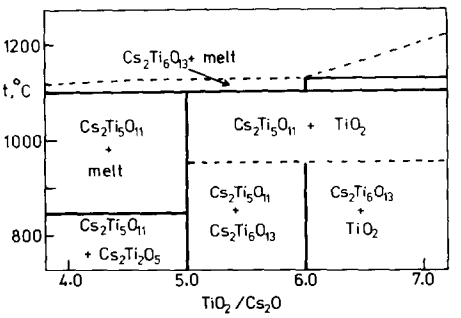

FIG. 1. Partial phase diagram for Cs_2O–TiO_2. The phase boundary at the eutectic temperature of 844°C is from Ref. (*6*).

Results and Discussion

Phase Studies

The results of the phase analysis in air are summarized in Fig. 1. Compositions with $Cs_2O:TiO_2$ ratios in the range 1:3–1:8 were reacted in the temperature range 850–1200°C. Two new titanate phases were identified, with $Cs_2O:TiO_2$ ratios of 1:5 1:6, i.e., $Cs_2Ti_5O_{11}$ and $Cs_2Ti_6O_{13}$. The former compound formed asbestos-like fibrous crystals whereas the latter compound occurred as very thin transparent flakes with a pronounced micaceous cleavage. For ease of description we will refer to them as needle and platelet phases, respectively.

At temperatures below the solidus line, the platelet phase appeared to be metastable. Regrinding and reheating platelet phase samples gave mixtures of the needle phase plus rutile. The upper temperature limit for metastability of 950°C, shown in Fig. 1, is for samples that received a single heat treatment. The liquidus line was not determined accurately because of the problem of cesium volatilization. No evidence was found for the congruently melting phase

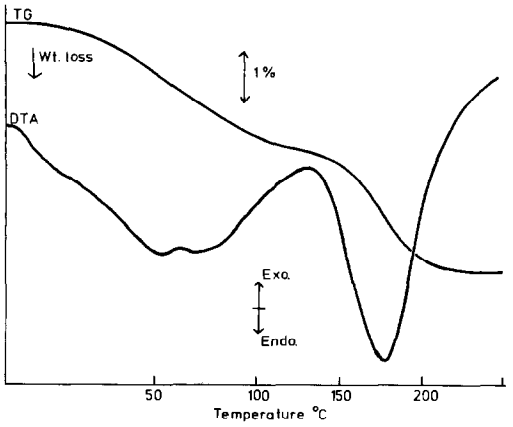

FIG. 2. TG/DTA curves for $Cs_2Ti_5O_{11} \cdot (1 + x)H_2O$.

$Cs_2Ti_4O_9$, reported by Schmitz-DuMont and Reckhard (*6*). At temperatures below 1115°C, samples at this composition gave mixtures of the needle phase plus a quenched liquid phase, and above 1115°C, a mixture of the platelet phase plus liquid.

Reactions of CsOH + TiO_2 mixtures in sealed platinum tubes gave similar results, except that black crystals of a cesium hollandite phase (*7*) were observed in samples with $Cs_2O : TiO_2$ ratios greater than 1 : 6.

Hydration of the Needle Phase

The needle phase was found to undergo a reversible hydration reaction below 200°C, accompanied by significant changes of the *d*-spacings of many reflections in the powder pattern. The dehydration reaction was studied by TG/DTA methods. The results are shown in Fig. 2. Two overlapping dehydration steps were observed at 25–130 and 130–270°C. The DTA curve for the first step comprised two broad, overlapping endotherms at 55–60 and 75–80°C whereas that for the second step comprised a single sharp endotherm at 170–175°C. For different samples, the total weight loss varied between 4.1 and 5.2 wt%, being divided approximately equally between the two steps. The loss of 1 mole of water per $Cs_2Ti_5O_{11}$ formula weight would correspond to a weight loss of 2.6 wt%. The composition of the hydrated phase is thus $Cs_2Ti_5O_{11} \cdot (1 + x)H_2O$, with x in the range 0.5–1.

The infrared spectrum of the hydrated needle phase in the range 4000–1000 cm^{-1} comprised sharp peaks at 3340, 3080, and 1690 cm^{-1} overlying broader peaks at ~3400 and 1640 cm^{-1}. The latter peaks correspond to stretching and bending modes of water. The series of sharp peaks may be interpreted as due to OH^- and H_3O^+. For comparison, ν(OH) for the amphoteric oxydroxides, lepidocrocite and boehmite, occur at 3390, 3125 and 3297, 3090 cm^{-1}, respectively (*8, 9*). The bending frequency ($\nu 4$) of H_3O^+ is reported to occur in the range 1570–1750 cm^{-1} (*10*), cf 1690 cm^{-1} observed. The stretching frequencies of the oxonium ion ($\nu 1$, $\nu 3$) overlap those of ν(OH) and $\nu 1$, $\nu 3(H_2O)$ near 3400 cm^{-1}.

Structural Studies

(*i*) *Platelet phase.* Single-crystal diffraction patterns for the platelet phase displayed body-centered orthorhombic symmetry. Lattice parameters obtained from a

TABLE I

X-RAY POWDER DIFFRACTION DATA: $Cs_2Ti_6O_{13}$

h k l	d_{calc} (Å)	d_{obs} (Å)	*I*
0 2 0	8.64	8.61	11
0 4 0	4.318	4.328	20
1 1 0	3.735	3.737	2
1 3 0	3.186	3.190	100
0 1 1	2.919	2.921	8
0 6 0	2.879	2.879	15
0 3 1	2.633	2.629	2
1 5 0	2.564	2.564	4
1 2 1	2.260	2.251	21
0 5 1	2.248		
1 7 0	2.073	2.072	3
2 0 0	1.913	1.912	17
0 10 0	1.727	1.727	3
1 9 0	1.715	1.714	3
2 1 1	1.600	1.591	9
1 8 1	1.587		
0 0 2	1.481	1.481	4

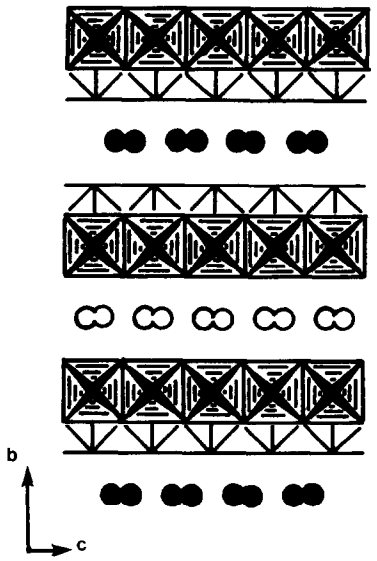

FIG. 3. Polyhedral representation of the average structure in space group *Immm* for $Cs_2Ti_6O_{13}$ viewed along *a*. The open circles represent Cs at $x = 0$ and filled circles are Cs at $x = \frac{1}{2}$. Split pairs of Cs atoms are separated by 0.8 Å along *c*.

powder pattern (Table I) refinement are $a = 3.825(2)$, $b = 17.271(7)$, $c = 2.961(1)$ Å (for material prepared at 800°C). The compound is isostructural with $Cs_xMg_{x/2}Ti_{2-x/2}O_4$ (*11*), which has a structure based on corrugated layers of edge- and corner-shared octahedra parallel to (010) with cesium ions packing between the layers in eight-coordinated sites (see Fig. 3).

The platelet phase differs from other reported layer structures of this type in that the positive charge of the interlayer cations is not balanced by partial replacement of Ti^{4+} by M^{2+} or M^{3+} in the octahedral layers. Two alternative charge-compensation mechanisms are possible: titanium vacancies or incorporation of neutral Cs_2O in the interlayer region. The latter model is consistent with the observed micaceous cleavage parallel to (010), and has been confirmed by a structure refinement (to be published).

Long-exposure precession photographs showed diffuse diffraction effects, in the form of continuous streaks parallel to *g* (010). The intersection of the streaks with the a^*c^* plane occurred at multiples of $\frac{1}{2}g$ (100) and $\frac{1}{3}g$ (001), corresponding to a superstructure, $a = 2a_0$, $b = b$, $c = 3c_0$. These diffuse reflections appear as broad humps in the powder pattern, with large integrated intensities, indicating they are due to an ordering of cesium ions. The relatively small cross section of the streaks indicates that the intralayer ordering is well developed, but there is little correlation from one layer to the next. Studies on the intralayer cesium ordering are in progress.

TABLE II

X-RAY POWDER DIFFRACTION DATA: $Cs_2Ti_5O_{11} \cdot (1 + x)H_2O$

h k l	d_{calc} (Å)	d_{obs} (Å)	*I*
2 0 0	10.19	10.15	14
2 0 1	6.486	6.492	15
4 0 $\bar{2}$	5.665	5.655	12
2 0 $\bar{3}$	4.937	4.939	50
4 0 $\bar{3}$	4.666	4.663	10
0 0 3	4.250	4.246	19
4 0 1	4.061	4.062	37
6 0 $\bar{2}$	3.974	3.974	26
6 0 $\bar{1}$	3.812	3.805	6
1 1 0	3.736	3.731	10
2 0 3	3.353	3.348	22
3 1 0	3.317	3.315	78
0 0 4	3.187	3.192	7
3 1 1	3.029	3.029	75
1 1 $\bar{3}$	2.949	2.952	100
5 1 $\bar{1}$	2.942		
6 0 1	2.928	2.935	78
6 0 $\bar{5}$	2.880	2.884	17
2 0 $\bar{5}$	2.846	2.844	50
8 0 $\bar{4}$	2.833		
1 1 3	2.682	2.681	28
3 1 $\bar{2}$	2.678		
5 1 $\bar{4}$	2.600	2.601	24
7 1 $\bar{2}$	2.533	2.536	29
10 0 $\bar{4}$	2.362	2.361	29
7 1 $\bar{5}$	2.230	2.230	22
7 1 1	2.12	2.125	54
0 0 6	2.125		
12 0 $\bar{3}$	1.968	1.968	7
0 2 0	1.900	1.900	39

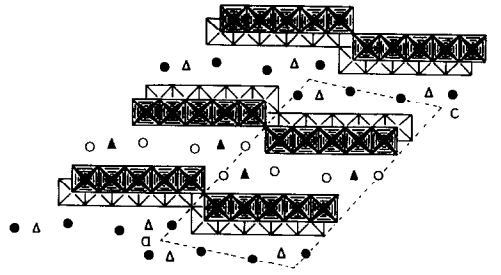

FIG. 4. Polyhedral representation of the structure for $Cs_2Ti_5O_{11} \cdot (1 + x)H_2O$, viewed along *b*. The open circles and triangles represent Cs and H_2O, respectively, at $y = 0$. Filled circles and triangles correspond to atoms at $y = \frac{1}{2}$.

(*ii*) *Hydrated needle phase.* Weissenberg and precession photographs showed face-centered monoclinic symmetry, with possible space groups *C*2/*m*, *Cm*, or *C*2. The indexed powder pattern is given in Table II. Refined cell parameters are $a = 23.849(8)$, $b = 3.800(1)$, $c = 14.918(6)$ Å, $\beta = 121.27(3)°$.

The structure of the hydrated needle phase has been determined and the model refined in space group *C*2/*m*, using powder data and a modified Rietveld profile refinement program. Details will be reported elsewhere. A polyhedral representation of the structure, viewed in projection down *b*, is shown in Fig. 4. The close relationship to the layer structure of the platelet phase, Fig. 3, is obvious. In the needle phase, the corrugated layers are periodically stepped to give ribbons 5-octahedra wide, which are linked via corner-sharing of the octahedra. Cesium ions and H_2O (or H_3O^+,OH^-) occupy the interlayer region, with an eclipsed stepping of the cesium ions in the regions where the octahedral framework steps, The unit cell composition determined from the structure refinement is $4 \times Cs_2Ti_5O_{11} \cdot H_2O$. The extra water was not located and is presumably distributed over a number of sites in the interlayer region.

(*iii*) *Dehydrated needle phase.* This phase has the same symmetry and space group as the hydrated compound. Its powder pattern is given in Table III. Refined cell parameters are $a = 19.719(8)$, $b = 3.808(1)$, $c = 15.023(6)$ Å, $\beta = 106.93(3)°$. The structure has been determined and refined using powder data (collected at 200°C). The model is shown in projection down *b* in Fig. 5. From

TABLE III

X-RAY DIFFRACTION DATA:[a] $Cs_2Ti_5O_{11}$

h k l	d_{calc} (Å)	d_{obs} (Å)	*I*
2 0 0	9.43	9.45	9
2 0 $\bar{3}$	4.884	4.887	10
4 0 0	4.710	4.716	6
4 0 $\bar{1}$	4.138	4.141	50
4 0 $\bar{3}$	3.992	3.999	8
1 1 0	3.733	3.737	14
0 0 4	3.593	3.591	10
3 1 0	3.258	3.256	100
3 1 1	3.078	3.077	93
6 0 $\bar{1}$	2.900	2.898	82
3 1 $\bar{3}$	2.905	2.900	36
6 0 $\bar{4}$	2.805	2.808	28
3 1 $\bar{4}$	2.618	2.619	11
8 0 $\bar{4}$	2.303	2.304	21
7 1 $\bar{1}$	2.256	2.253	9
3 1 4	2.250		
5 1 $\bar{5}$	2.200	2.201	9
2 0 6	2.175	2.175	28
0 2 0	1.904	1.904	48
10 0 2	1.707	1.706	9

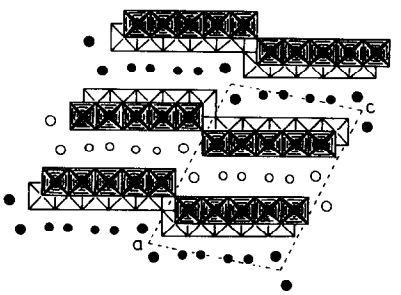

FIG. 5. Polyhedral representation of the structure for $Cs_2Ti_5O_{11}$ viewed along *b*. The open circles represent partially occupied Cs sites at $y = 0$ and filled circles are Cs at $y = \frac{1}{2}$. Areas of circles are proportional to occupancies.

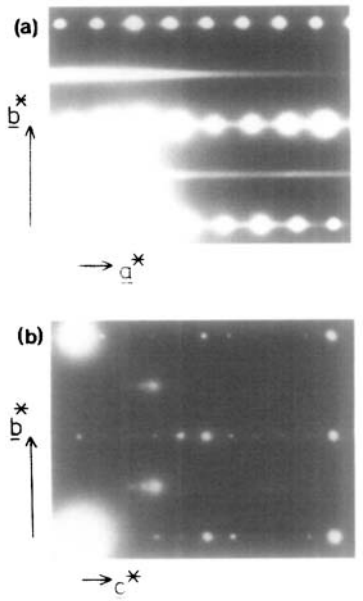

FIG. 6. (a) [001] zone axis electron diffraction pattern for $Cs_2Ti_5O_{11}$, showing streaking along a^* for rows having half-integral multiples of b^*. (b) [100] zone axis pattern showing superlattice reflections requiring a doubling of both b and c.

a comparison with Fig. 4, it is apparent that the removal of water is accompanied by a sliding of the layers relative to one another, resulting in a net displacement of 1.5 octahedra parallel to the layers, while maintaining the same separation perpendicular to the layers.

Unlike the hydrated phase, in which the cesium ions are fully ordered, the dehydrated phase has only short-range ordering of the large cations. A statistical distribution of cesiums over a number of partially occupied sites was established from the refinement. Electron diffraction patterns displayed diffuse scattering for reciprocal lattice rows having half-integral multiples of b^*. Thus [001] zone axis patterns showed continuous diffuse streaking along a^* (Fig. 6a), whereas [100] patterns showed superlattice relections (i.e., streaks viewed in cross section) requiring a doubling of both b and c axes (Fig. 6b). By analogy with the platelet phase, these are due to intralayer ordering of cesium ions, with little or no correlation between the ordering in successive interlayer regions. The model shown in Fig. 5 represents the average distribution of cesium ions.

The dehydrated needle phase, $Cs_5Ti_5O_{11}$, is the first reported example of an $n = 5$ member of the stepped-layer series for which many $n = 4$ members, $A_2Ti_4O_9$, A = Li, Na, K, Rb, Cs, Tl, Ag, are known (*12, 13*). Samples of the needle phase prepared from CsOH + TiO_2 mixtures in sealed platinum tubes (~2 atm pressure) gave single-crystal diffraction patterns corresponding to intergrowth structures between $n = 5$ and $n = 6$ members, suggesting that at higher pressures, the $n = 6$ member may be stable, cf. the reported preparation of an asbestos-like titanate phase of composition $Cs_2Ti_6O_{13}$ at a pressure of 200 atm (*14*).

Acknowledgments

We are grateful to Dr. J. Hamilton for making available the Stanton-Redcroft thermobalance. We thank also Mr. N. Davies and the Central Resource Laboratory, University of Tasmania, for the FTIR measurements, and Dr. David Smith, Cambridge, U.K., for Fig. 6a.

References

1. A. G. SOLOMAH, R., ODOJ, AND C. FREIBURG, *J. Amer. Ceram. Soc.* **67,** C-50, (1984).
2. E. R. VANCE AND D. K. AGARWAL, *Nucl. Chem. Waste Manage.* **3,** 229 (1982).
3. R. CHEARY AND J. KWIATKOWSKA, *J. Nucl. Mater.* **125,** 236 (1984).
4. L. A. BURSILL AND J. KWIATKOWSKA, *J. Solid State Chem.* **52,** 45 (1984).
5. A. E. RINGWOOD, "Safe Disposal of High Level Nuclear Reactor Waste: A New Strategy," Australian National University, Canberra, Australia (1978).
6. O. SCHMITZ-DUMONT AND H. RECKHARD, *Monatsh. Chem.* **90,** 134 (1959).
7. M. LUNDBERG AND S. ANDERSSON, *Acta Chem. Scand.* **18,** 817 (1964).
8. J. J. FRIPIAT, H. BOSMANS, AND P. G. ROUXHET, *J. Phys. Chem.* **71,** 1097 (1967).

9. K. SATO, T. SUDO, F. KUROSAWA, AND O. KAMMORI, *Nippon Kinzoku Gakkaishi* **33,** 1371 (1969).
10. G. V. YUKHNEVICH, *Russ. Chem. Rev.* **32,** 619 (1963).
11. A. F. REID, W. G. MUMME, AND A. D. WADSLEY, *Acta Crystallogr. Sect. B* **24,** 1228 (1968).
12. A. VERBAERE AND M. TOURNOUX, *Bull. Soc. Chim. Fr.* **4,** 1237 (1973).
13. M. DION, Y. PIFFARD, AND M. TOURNOUX, *J. Inorg. Nucl. Chem.* **40,** 917 (1978).
14. T. E. GIER AND P. L. SALZBERG, U.S. Patent 2,833,620 (1958).